PERFORMANCE OF NITROGEN-DOPED 9-CELL SRF CAVITIES IN VERTICAL TESTS AT CORNELL UNIVERSITY*

M. Ge#, R. Eichhorn, B. Elmore, F. Furuta, D. Gonnella, T. Gruber, G. Hoffstaetter, J. Kaufman, M. Liepe, T. O'Connell, J. Sears, E. Smith, Cornell University, Ithaca, NY 14853, USA

Abstract

Cornell University treated five LCLS-II 9-cell cavities by nitrogen-doping recipe. In this paper, we reported the performance of these 9-cell cavities. In the treatments, the nitrogen recipes are slightly different. The cavities have been firstly doped under high nitrogen pressure; after the vertical tests some of the cavities has been reset the surface and re-doped under light nitrogen pressure. The detail of the cavity preparation and test results will be shown. The comparison of the different recipes will be discussed.

INTRODUCTION

The LCLS-II project [1] requires its Superconducting RF (SRF) cavities working at accelerating gradient (E_{acc}) 16MV/m with intrinsic quality factor (Q_0) 2.7×10^{10} at temperature 2K. The quality factor of a standard electro-polished (EP) cavity can achieve $1.5\text{-}2.5\times10^{10}$ at temperature 2K [2]. Therefore the EP'd cavities cannot reliably meet the requirement of LCLS-II. The nitrogen-doping recipe has been developed and applied for the LCLS-II project, which can reliably produce Anti-Q-slope for cavities [3-5]. Cornell University treated five 1.3GHz 9-cell SRF cavities for the LCLS-II project by the nitrogen-doping recipe. Both the light-doping and heavy-doping recipe has been applied to these cavities. The details of the treatments and vertical test results will be shown and discussed in the following sections.

CAVITY TREATMENTS

The cavities were received as a brand new cavity from Advanced Energy Systems, Inc. (AES), shown in Fig. 1 (a). The cavities have been vertical electro-polished (VEP) about 120μm by Cornell VEP system [6] (Fig. 1 (b)).

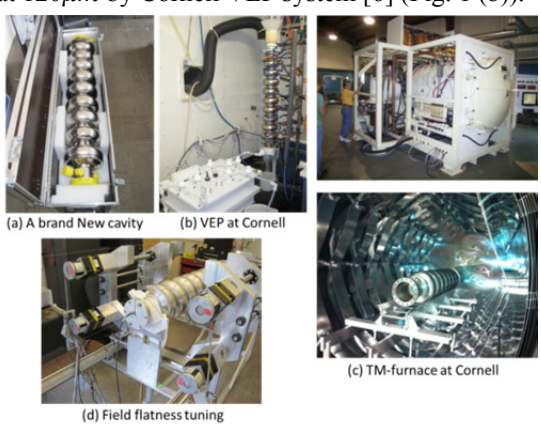

Figure 1: The photographs of the cavity treatments.

Then the cavities were baked in Cornell TM-furnace [7] (displayed in Fig. 1 (c)) at 800°C to degas hydrogen. Figure 2 shows the curves of the partial pressure versus time for the cavity TB9AES018. In total this cavity had been baked about 3 days. However, the curves manifest that the hydrogen can be degassed within 10 hours. Therefore we reduced the baking time to 3 hours for the rest cavities, because long time baking will soften the material and deform the cavities.

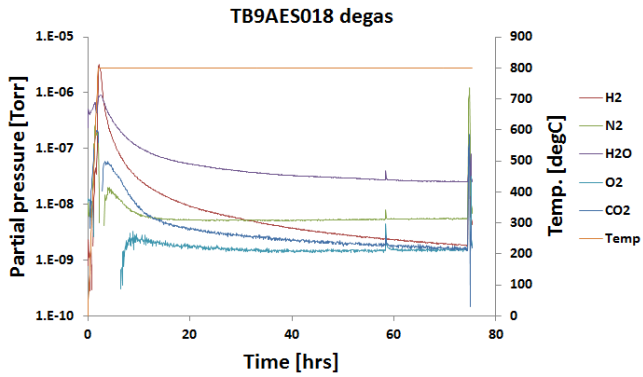

Figure 2: 800°C degassing curves of the cavity TB9AES018; On left scale: the partial pressure versus time curves; On right scale: the temperature versus time curve.

At the end of the baking, high pure nitrogen gas had been injected into the chamber of the furnace for doping; after the doping, the nitrogen gas was pumped out, and the cavity was kept 800°C under good vacuum for a while.

We treated the cavities in two runs: All five cavities had been doped with the heavy doping recipe and tested. After the first run two cavities had been reset the surface by bulk VEP, doped with light-doping recipe, and re-tested. The nitrogen pressure of the heavy and light recipes are listed as follow,

- The heavy doping: nitrogen pressure 40-60mTorr;
- The light doping: nitrogen pressure 20-30mTorr.

Figure 3 shows an example of the relation of nitrogen pressure versus time of the heavy doping recipe for the cavity TB9AES018. During the doping, the nitrogen pressure was difficult to be maintained at a constant level. Hence in our case, the pressure was oscillated in about 20mTorr ranges for both recipes. When the doping was completed, the cavities were tuned to keep field flatness better than 90%, shown in Fig. 1 (d).

*Work supported by the US DOE, the LCLS-II High Q0 Program, and NSF Grant NSF-PHY-1416318.
#mg574@cornell.edu

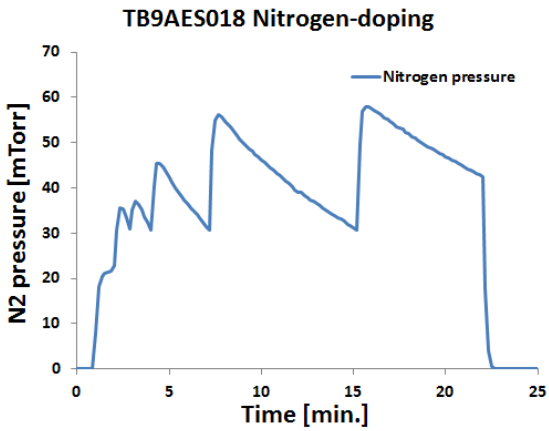

Figure 3: TB9AES018 nitrogen pressure versus time curve with heavy doping recipe.

The final removal of light VEP after the nitrogen doping affects the Q-value as well. Because too much removal will degrade the doping effects, but too less removal cannot remove surface contaminations. In reference [8], it lists the final removals and the Q_0 of single-cell and some of the 9-cell cavities. The cavities had been high-pressure water rinsed (HPR) and clean assembled in clean room before the vertical tests. The test results will be shown in next sections. When the vertical tests completed, all the five cavities had been sent back to Fermilab to address helium tank, after which they have been delivered to J-lab, Cornell and Fermilab for horizontal tests [5, 9, and 10].

During the light VEP, the inner surface layer of the HOM dampers peeled off from three 9-cell cavities, which caused huge amount of flakes coming into the cavities. Additional BCP on the HOM dampers as well as light VEP had been implemented for those cavities. The EDS and SEM analysis manifest that the materials of the flakes are Al, Si, *etc*.

VERTICAL TESTS

Tests Set-up

Before the vertical tests, the cavities had been mounted on the Cornell multi-cell insert, shown in Fig. 4, a serious of instruments: three Cernox temperature sensors, two Fluxgate magnetic-field probes, sixteen OST sensors, and multi-cell temperature-mapping system. The cavity has been set vertically; the main coupler port was on the bottom side. The Cernox sensors had been mounted on the top, middle, and bottom cells displayed in Fig. 4 to monitor thermal gradients during cool down and calibrate the T-Map. The OST sensors, for quenching detections, had been installed surrounding the cavity, the position of which is exhibited by the red points in Fig. 4. The fluxgate is used to measure DC magnetic-fields in Dewar during the cool down. One fluxgate measures the field perpendicular to the cavity beam axis which is caused by thermal currents; the other one capture the field parallel to the cavity beam axis which is the residual magnetic field. The T-map covers the middle 7-cell of a 9-cell cavity, which is able to measure the cooling front and detect quench locations.

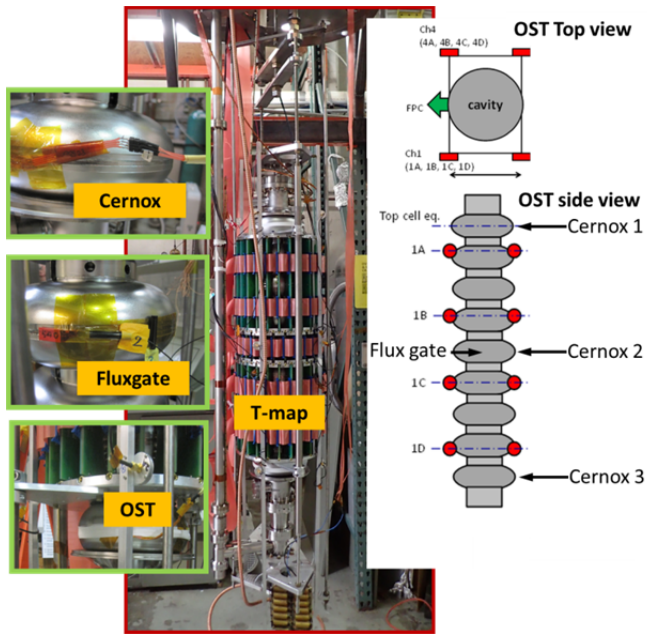

Figure 4: Vertical tests set-up with the Cernox sensors, the OST sensors, the flux gate, temperature-mapping system.

Cool down Speed

The cooling speed significantly affects residual resistance [11-13]. For the nitrogen-doped cavities, the fast cooling down generates the lower residual resistance to achieve higher Q-value [12]. Hence in all vertical tests, we implemented the fast cool down. Fig. 5 shows the temperature of the cavity TB9AES018 versus time when the cavity passed the critical temperature 9.2K. The calculation reveals that the cooling speed is 2.7K/min.

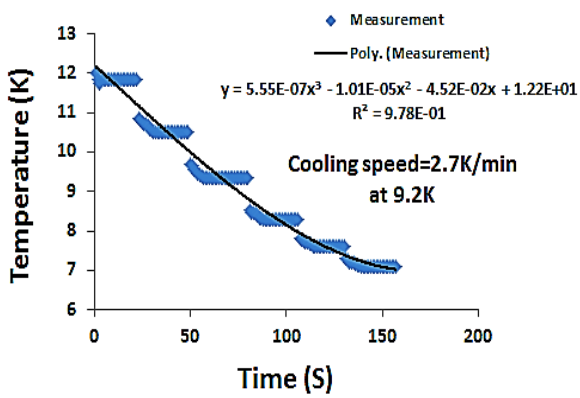

Figure 5: The cooling curve of cavity TB9AES018 when the cavity passed the critical temperature 9.2K.

The residual magnetic field had been measured during the cavities cooling down. Fig. 6 displays the measurement results of the cavity TB9AES018. When the cavity was passing T_c, the magnitude of the magnetic

ISBN 978-3-95450-178-6

field perpendicular to the cavity beam axis decreased from 0.0003Gauss to 0.001Gauss shown in Fig. 6 (a); while the magnitude of the magnetic field parallel to the beam axis jumped up to 0.002Gauss shown in Fig. 6 (b). The change of the field perpendicular to the beam axis relates the thermal current generated by the temperature gradient during the cool down; the jump of the parallel field is due to the Meissner effect of a superconductor. All the cool-downs in vertical tests are same; the residual magnetic fields were controlled under the tiny level (<5mGauss).

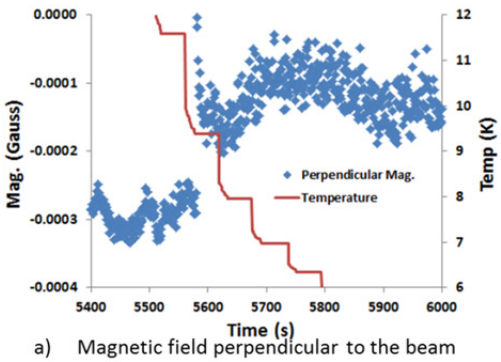

a) Magnetic field perpendicular to the beam axis, when the cavity passing the Tc.

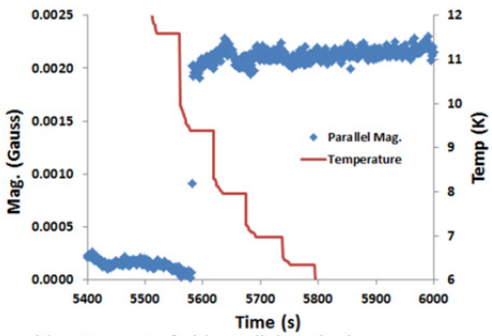

b) Magnetic field parallel to the beam axis, when the cavity passing the Tc.

Figure 6: The residual magnetic field when the cavity TB9AES018 passing the critical temperature 9.2K.

RF Measurement Results

The best vertical-test results at temperature 2K have been displayed in Fig. 7. The average Q_0 at 16MV/m is $3.0 \pm 0.3 \times 10^{10}$, the quench field is 17 ± 3MV/m. The results achieved the LCLS-II specification, *i.e.* Q_0=2.7×10^{10}at E_{acc}=16MV/m under temperature 2K.

Table 1 lists the summary of the detail results of the tests. In the first pass, the cavities had been treated by the heavy doping recipe, the Q-value of which achieved the specification. But the quench field is so closed to the specification. We reset the surface of the cavities TB9AES030 and TB9AES022 by ~40μmVEP; then re-doped by the light-doping recipe to improve the quench field further. The quench field of TB9AES030 has been improved about 5MV/m; but for TB9AES022, the result is even worse. The quench-location detection will be discussed in the next section. In general, the N_2-doping will cause the quench field lower than the EP'd cavities. But for the N_2-doped single-cell cavity, the quench field is higher than the 9-cell [8], which implies there is still a margin of the recipe optimization. Except the cavity TB9AES022, the quench region is featureless from the optical inspection. The mechanism of the low quench-field caused by the N_2-doping is unclear and under investigation.

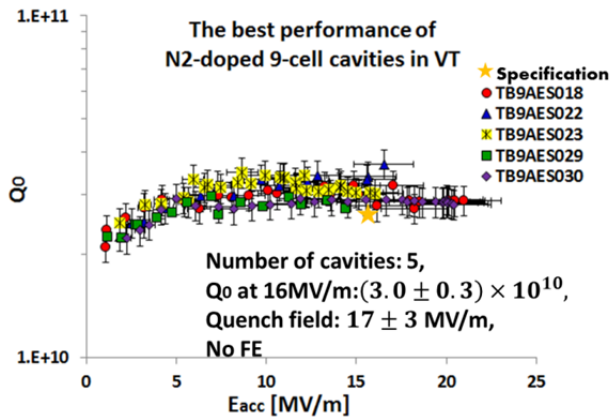

Figure 7: The summary of the best performance of the N2-doped cavities in vertical tests at temperature 2K.

Table 1: The Summary of VT of the N_2-doped Cavities

Cavity ID	1st Pass		2nd Pass	
	Q_0 at 16MV/m ($\times 10^{10}$)	Quench field (MV/m)	Q_0 at 16MV/m ($\times 10^{10}$)	Quench field (MV/m)
TB9AES018	3.2	22	-	-
TB9AES022	3.2	16	2.0 (at quench)	15
TB9AES023	2.9	16.1	-	-
TB9AES029	2.7 (at quench)	14.5	-	-
TB9AES030	2.7	17	2.8	22.3

DATA ANALYSIS

Quench Detection by T-Map, OST, and Optical Inspection

As it described in the previous section, the cavity TB9AES022 equipped with the T-map [14] and OST systems [15] shown in Fig. 4 during the VTs. Figure 8 displays the quench location and the quench signal detected by the instruments. The OST system and T-Map showed the consistent quench location of TB9AES022. The quench happened on the equator region of the 8th cell counted from the bottom. The T-map captured the quench pulse shown in Fig. 8 as well. The T-map monitors the resistance value of each sensor; when the quench happens, the temperature of the quench spot will suddenly increase, which will cause the T-map sensor resistance dropping. The T-map is able to record the resistance versus time curves on the quench spot; hence it can obtain the temperature versus time curves of the quench after converting the resistance value to temperature by calibrations. The quench pulse in Fig. 8 suggests that the temperature of the quench spot jumped from 2K to 17K, the pulse width is about 350ms. No pre-heating was observed.

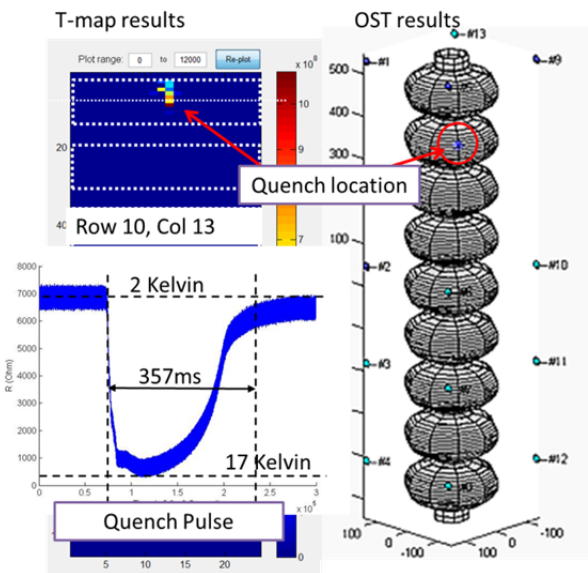

Figure 8: Quench location of TB9AES022 detected by the OST and T-map system; The quench pulse recorded by T-map system.

The quench location has been inspected by the Cornell inspection system; the defect was observed. Figure 9 a) is the defect location indicated by the red laser point from the outside of the cavity. Figure 9 b) shows the inspection image of the defect, the radius of which is about 500μm. The defect located a little bit away from the welding seam but within the heat affect zone. The surface replica has been made to extract 3-D profile of the defect shown in Fig. 9 c) [16]. Fermilab scanned the feature and determine the defect is a bump but not a pit. The 3D-profile sliced along the equator direction is exhibited in Fig. 9 d). The height of the bump is about 140 μm. This feature might be the welding bead attached during the cavity electron beam welding. This feature can be removed by local mechanical polishing.

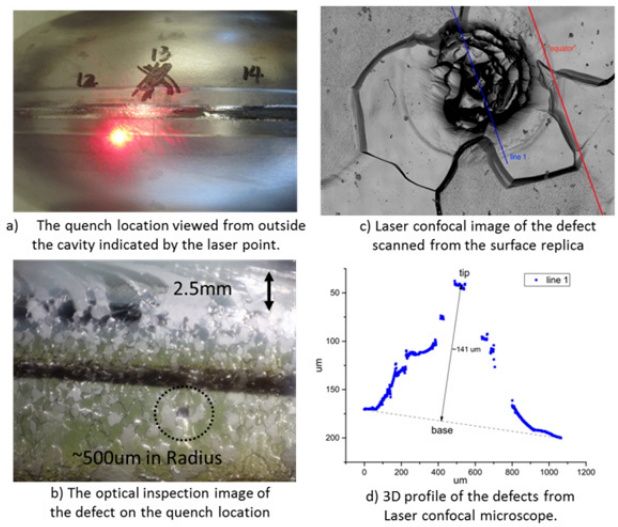

Figure 9: The defect observed on quench location of TB9AES022 by inspection system and surface replica.

The BCS Resistance and Residual Resistance

The BCS resistance R_{BCS} and residual resistance R_0 versus field can be extracted by the method described in the references [17-18]. The results have been listed in Table 2. The R_{BCS} and R_0 can be affected by the amount of final VEP removals as well as the doping recipes. The VEP removal amount has been decided based on the single-cell studies [8] and communications between FNAL, J-Lab [10]. The VEP amount had firstly been set 14$\mu m$for heavy doping; but most cavities had been VEP'd around 20-30 μm due to the flake issue and field emission. The small amount of additional removal does not affect the R_{BCS} and R_0 significantly. At E_{acc} 16MV/m, the R_{BCS} at temperature 2K is around 6-7.5$n\Omega$; the R_0 is around 2-3$n\Omega$. The light-doping does not affect the R_{BCS} and R_0; hence the Q-value of the light-doped cavity is quite similar to the heavy-doped cavities. But the light-doping only improved the quench field.

ISBN 978-3-95450-178-6

Table 2: The R_{BCS} and R_0 Summary of the N_2-doped Cavities

Cavity ID	Recipe	Final VEP removal (μm)	$R_{BCS}(n\Omega)$ at 16MV/m, 2Kelvin	$R_0(n\Omega)$ at 16MV/m
TB9AES018	Heavy-doped	24	7.0	2.3
TB9AES022	Heavy-doped	14	5.9	2.6
TB9AES023	Heavy-doped	27	7.3	2.3
TB9AES029	Heavy-doped	27	7.9 (at quench)	2.6 (at quench)
TB9AES030	Heavy-doped	26	7.3	2.2
TB9AES022	Light-doped	5	6.5 (at quench)	2.3 (at quench)
TB9AES030	Light-doped	14	7.1	3.5

CONCLUSION

The five LCLS-II 9-cell cavities had been treated by N_2-doping recipe. The average performance of these cavities achieved the LCLS-II specification. The defect has been observed in the quench location of TB9AES022. Rest of cavities have featureless quench location. The defect has been analysed the surface replica technique. The BCS resistance and residual resistance have been analysed.

ACKNOWLEDGEMENT

We are grateful to Y. Trenikhina, G. Wu, and A. Romanenko from Fermilab for extracting the 3D profile of the defect in the cavity TB9AES022.

REFERENCES

[1] J.N. Galayda. "The Linac Coherent Light Source-II project", TUOCA01, Proceedings of IPAC2014, Dresden, Germany, 2014.
[2] H. Padamsee, "RF Superconductivity, Vol. II Science, Technology, and Applications", WILE-VCH, 2009.
[3] A. Grassellino, *et, al.*, Nitrogen and argon doping of niobium for superconducting radio frequency cavities: a pathway to highly efficient accelerating structures, Supercond. Sci. Technol. **26**, 102001 (2013).
[4] D. Gonnella, *et, al.*, "New Insights into Heat Treatment of SRF Cavities in a Low-pressure Nitrogen Atmosphere", WEPRI064, Proceedings of IPAC2014, Dresden, Germany (2014).
[5] D. Gonnella, *et al.*, "Nitrogen-doped 9-cell cavity performance in a test cryomodule for LCLS-II", J. Appl. Phys. 117, 023908 (2015).
[6] F. Furuta, *et. al.*, 'Vertical Electro-Polishing studies at Cornell', MOPB093, in this conference, SRF'15, Whistler, Canada (2015).
[7] F. Furuta, *et al.*, "TM-Furnace qualification at Cornell", TUP059, Proceedings of SRF2013, Paris, France (2013).
[8] D. Gonnella, *et al.*, 'Nitrogen treated cavity testing at Cornell', THPP016, Proceedings of LINAC 2014, Geneva, Switzerland, (2014).
[9] A. Hocker, *et al.*, "Continuous-wave horizontal tests of dressed 1.3GHz SRF cavities for LCLS-II", MOPP054, Proceedings of LINAC2014, Geneva, Switzerland (2014).
[10] M. Liepe, *et al*. "The Joint High Q0 Program for LCLS-II", WEPRI062, Proceedings of IPAC 14, Dresden, Germany, 2014.
[11] J.-M. Vogt, *et al.*, "Impact of cool-down conditions at Tc on the superconducting rf cavity quality factor", Phys. Rev. Sp. Top. – Acc. And Beams 16 (2013)102002.
[12] A. Romanenko, *et, al.*, "Dependence of the residual surface resistance of SRF cavities on the cooling rate through Tc", arXiv:1401.7747.
[13] R. Eichhorn, *et, al.*, "Thermo-currents and their Role in high Q Cavity Performance", arXiv:1411.5285v2.
[14] F. Furuta, *et al.*, "Multi-cell T-mapping and conclusions", TUPB081, in this conference, SRF'15, Whistler, Canada (2015).
[15] A. Ganshin, *et al.,* "Temperature waves in SRF research", TUP104, Proceedings of SRF2013, Paris, France (2013).
[16] M. Ge, *et al.*, "Routine characterization of 3D profiles of SRF cavity defects using replica techniques", Supercond. Sci. Technol. 2011, 24, 035002.
[17] A. Romanenko, *et, al.*, "Dependence of the microwave surface resistance of superconducting niobium on the magnitude of the rf field", Appl.Phys.Lett. 102 (2013) 252603.
[18] M. Ge, *et, al*., "Field-dependent surface resistance of a superconducting RF cavity caused by surface impurity", arXiv:1507.08704v2.